Short Title: BET Proteins and Replication Stress in Cancer

Interplay between BET Proteins and the Pre-Replication Complex Unveils Therapeutic Vulnerabilities in Cancer

Kai Doberstein[1,2,*], Vivica Messner[1], Sebastian Berlit[1], Benjamin Tuschy[1], Marc Sütterlin[1,2], Frederik Marmé[1,2,3]

[1]Department of Obstetrics and Gynaecology, Medical Faculty Mannheim of the Heidelberg University, University Medical Centre Mannheim, 68167 Mannheim, Germany.
[2]Mannheim Institute for Innate Immunoscience, Medical Faculty Mannheim of the Heidelberg University, 68167 Mannheim, Germany.
[3]DKFZ-Hector Cancer Institute at University Medical Center Mannheim, Mannheim, Germany.

*Corresponding Author: Kai Doberstein, kai.doberstein@medma.uni-heidelberg.de

Keywords: BET proteins, replication stress, TP53, ovarian cancer, AZD5153, XL413

Abbreviations: BET (bromodomain and extraterminal), pre-RC (pre-replication complex), HGSC (high-grade serous ovarian carcinoma), CDC7 (cell division cycle 7), MCM (minichromosome maintenance), R-loop (RNA-DNA hybrid), DSB (double-strand break), HR (homologous recombination).

Novelty and Impact: This study reveals a synthetic lethal interaction between BET inhibitors and CDC7 inhibition in TP53-mutated cancers, particularly high-grade serous ovarian carcinomas. By inducing unresolved DNA damage and R-loop accumulation, this combination therapy offers a novel strategy to exploit replication stress in cancer, with potential clinical implications for targeted therapy.

Abstract:

Replication stress is a critical event in cancer development and understanding the underlying molecular mechanisms can help to identify new treatment strategies. Here, we investigate the molecular interplay between the pre-replication complex (pre-RC) and the bromodomain and extraterminal domain (BET) proteins in orchestrating replication stress response. Our findings reveal a mutual dependency between BET proteins and the pre-RC within cancer cells. Notably, reduction in origin licensing or replication initiation makes cells more susceptible to the BET-inhibitor AZD5153. Furthermore, we observe synergistic effects when combining the CDC7 inhibitor XL413 with AZD5153, effects which were partly dependent on *TP53* mutation status. This combination treatment results in unresolved DNA damage and R-loop formation, leading to increased genomic instability. These insights pave the way for novel strategies for targeted cancer therapies and provide a foundation for further investigation into the interplay between CDC7 and BET proteins in replication stress response.

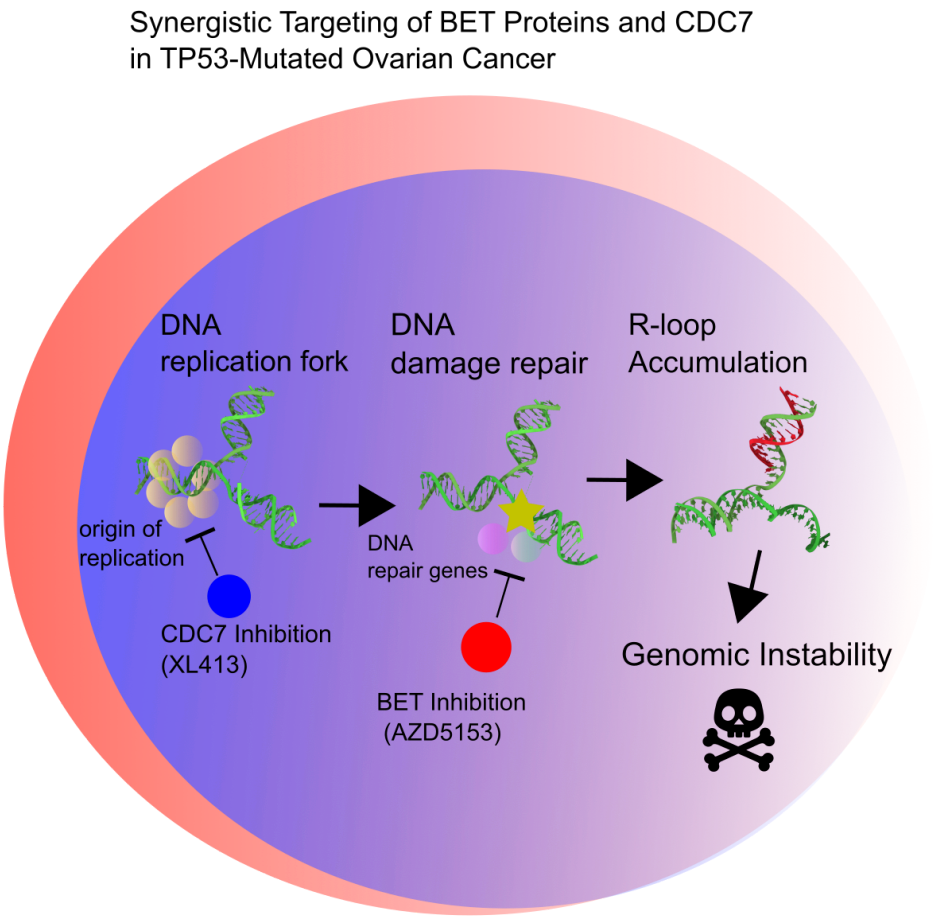

Graphical abstract: The graphic illustrates how the CDC7 inhibitor XL413 and the BET inhibitor AZD5153 work together in TP53-deficient cancer cells. First, XL413 prevents activation of the origin of replication complex, leading to DNA damage. Second, the DNA repair machinery is unable to resolve this damage, resulting in the accumulation of unresolved R-loops and genomic instability. Ultimately, this cascade culminates in cell death.

Introduction:

BET proteins are a family of transcriptional co-regulators that play a crucial role in modulating gene expression. This family includes four members: BRD2, BRD3, BRD4, and BRDT. All BET proteins feature two N-terminal conserved tandem bromodomains and a C-terminal extraterminal domain, both of which are essential for their functionality[1]. The bromodomain binds to acetylated lysine residues on histone proteins, while the extraterminal domain interacts with transcriptional activators, such as P-TEFb, allowing the BET proteins to regulate gene expression[2].

BET proteins are implicated in various biological processes, including cell cycle regulation, DNA repair, and embryonic development[3–6]. Among the BET proteins, BRD4 stands out as a key regulator of gene expression[7]. It actively participates in chromatin remodeling and transcriptional regulation, influencing multiple genes through direct interaction or by recruiting other proteins that can promote or inhibit gene expression[8,9,10]. Given its role in regulating oncogenes like *MYC*, BRD4 has been associated with cancer development, making it an attractive therapeutic target[11]. BET-inhibitors have shown promise in treating cancer and inflammatory diseases, with the first BET-inhibitor, JQ1, demonstrating the capacity to reduce tumor growth both *in vitro* and *in vivo*[12]. Other BET-inhibitors, such as I-BET151 and CPI-0610, have also shown potential in preclinical trials as anti-tumor and anti-inflammatory agents in preclinical studies[13].

In ovarian cancer, BET-inhibitors have been shown to decrease the growth of cancer cells, induce replication stress and increase the sensitivity to PARP inhibitors[14]. Several BET-inhibitors have been developed and evaluated in preclinical and clinical trials[15], demonstrating promise in reducing ovarian cancer cell proliferation and preventing disease progression, while exhibiting tolerable side effects. For instance, JQ1 significantly reduced the growth of ovarian cancer cells, decreased cancer spread and improved overall survival in mouse models[16].

Furthermore, BRD4 has been implicated in the recruitment and stabilization of replication proteins at the DNA replication fork[4,17,18]. By interacting with CDC6, PCNA and MCM7, BRD4 plays a pivotal role in the assembly and function of the replication initiation complex[4,19].

In this study, we elucidate the intricate interplay between the BET proteins and the pre-replication complex in the context of replication stress response. By combining the BET-inhibitor AZD5153 with a reduction in origin licensing or replication initiation, we demonstrate a potent sensitization to treatment, underscoring the therapeutic potential of targeting both BET proteins and the replication processes.

Methods:

Bioinformatics:
Data from the TCGA Ovarian cancer cohort were obtained from the XENA portal (UCSC) and cBio-Portal. Expression and drug response data for cell lines were sourced from the Dependency Map portal (depmap.org). Synergies were calculated using SynergyFinder 2.0. Data analysis was performed in R, with graphical representations created using GraphPad Prism 7 and complex heatmap R packages.

Western Blot:
Cells were lysed in RIPA buffer with protease inhibitors, and protein concentration was quantified using the Bradford assay (Bio-Rad). Proteins (20 µg) were separated on a 4-15% SDS-PAGE gel, transferred to PVDF membranes (TurboBlot, Bio-Rad), and blocked with 5% BSA in TBS-Tween. Membranes were incubated with primary antibodies (Supplementary Table S1) overnight at 4°C, followed by HRP-conjugated secondary antibodies. Protein bands were detected using Clarity Chemiluminescent HRP Reagent (Bio-Rad) and visualized with a Fusion SL imaging system.

Cell Culture:
FT189, FT237, FT240, FT246, FT282, KURAMOCHI, OVCAR4, COV318, OVCAR8, and OVSAHO cells were provided by Ronny Drapkin (UPenn), while OVCAR3 and HEYA8 were obtained from ATCC. Cells were cultured in DMEM F12 (Invitrogen) supplemented with 10% FBS (Atlanta Biologicals) and 1% penicillin/streptomycin (Invitrogen) at 37°C with 5% CO_2.

Short-interfering RNA transfection
P53, MCM7, or CDT1 expression was downregulated using a pool of three siRNA duplexes (Trilencer-27, Origene), with scrambled siRNA as a negative control. Cells (1×10^5/well) were transfected 24 hours post-seeding using Lipofectamine RNAiMAX (Invitrogen) with 10 nM siRNA, following the manufacturer's protocol.

Cell Survival Assay:
Cell survival was assessed using the CellTiter 96® Non-Radioactive Cell Proliferation Assay (Promega) at 570 nm absorbance. Experiments were performed in triplicate and repeated three times. Data are presented as means ± SD, with statistical significance determined by ANOVA and post-hoc analysis. Crystal violet staining was used to count attached cells.

Immunofluorescence:
Cells grown in 96 well plates were fixed in 4% paraformaldehyde, permeabilized with 0.3% Triton X-100, and blocked using Superblock. Primary antibodies were incubated for 2 hours at room temperature or overnight at 4°C, followed by secondary antibodies conjugated to Alexa Fluor dyes (Molecular Probes). Nuclei were stained with DAPI, and cells were mounted with Fluoromount-G (Sigma-Aldrich). Imaging was performed using a Zeiss Axio Observer microscope (40x). Foci and nuclear intensity were quantified using Cell Profiler and ImageJ.

EdU Labeling:
Cells were pulsed with 10 μM EdU for 20 minutes, permeabilized with 0.5% Triton X-100, and developed using a cocktail containing Tris-buffered saline, $CuSO_4$, Sulfo-Cyanine 3 Azide, and Sodium Ascorbate. Cells were rinsed and analyzed.

Fiber Spread Assay:
Cells were labeled with CIdU (38 μM) for 30 minutes, washed, and incubated with IdU (250 μM) for 30 minutes. Cells were lysed on slides, fixed in methanol/acetic acid, and denatured in 2.5 M HCl. Primary antibodies (anti-BrdU/IdU and anti-BrdU/CIdU) were incubated overnight, followed by secondary antibodies (Alexa 488 and Cy3). Slides were mounted with Antifade Gold (Invitrogen) and analyzed using a Leica fluorescence microscope (100x) and ImageJ.

Cell Cycle Analysis:
Cells were fixed in ice-cold ethanol, stained with DAPI/Triton X-100 solution, and analyzed using a flow cytometer (355-450 nm).

Real-Time PCR:
RNA was isolated using the RNeasy Plus Mini Kit (Qiagen), reverse-transcribed to cDNA (RT2 Easy First Strand Kit, Qiagen), and quantified using POWERUP SYBR MASTER MIX (Life Technologies) on a QuantStudio Real-Time PCR system (Thermo Fisher). Gene expression was calculated using the ΔΔCt method. Primer sequences are listed in Supp. Table 2.

Results:

BET-inhibitor sensitivity and origin loading

Building on previous studies that highlighted an interaction between pre-replication complex (pre-RC) proteins and BET proteins, we investigated the potential of a mutual dependency between the pre-RC and BET gene expression[4,19]. We analyzed pre-RC and BET expression data from the TCGA ovarian cancer dataset revealing that patients clustered into two main distinct groups: those with low pre-RC expression (Cluster 1) and high pre-RC expression (Cluster 2) those with (Figure 1A). We found only a weak positive correlation between the expression of the individual BET genes and origin of replication genes. To better assess this relationship, we therefore generated a combined expression score for the BET genes *BRD2*, *BRD3*, *BRD4* and *BRDT*. We found that the BRD-high tumors exhibited significantly elevated levels of *MCM2*, *MCM3*, *MCM4*, *MCM7*, and *CDC7* compared to BRD-low tumors (Figure 1B). To determine if this co-expression indicates a mutual dependency, we examined the expression of origin of replication genes and the sensitivity to a panel of various BET-inhibitors from the PRISM dataset and the Cancer Cell Line Encyclopedia (CCLE) (Figure 1C)[20,21]. Similarly, to the TCGA data, we observed a positive correlation between the expression of pre-RC genes and BET genes (Figure 1D). Interestingly, while we did not observe a strong correlation between BET gene expression and BET-inhibitor sensitivity, we noted negative correlations between the expression of pre-RC genes and sensitivity to BET-inhibitor (Figure 1D, E). This negative correlation was observed for all six BET-inhibitors analyzed, but not when assessing the sensitivity to the loss of *BRD4* via CRISPR/CAS9. This suggests that cells with high pre-RC gene levels are more sensitive towards BET-inhibitors but not to the loss of *BRD4* itself. Interestingly, a previous study demonstrated that the BET homedomain inhibitor AZD5153 does not disrupt the pre-replication complex, unlike the loss of *BRD4*[19]. Moreover, the loss of *CDC7* by CRISPR/CAS9 showed a negative correlation with sensitivity to BET inhibitors, particularly with AZD5153 (Figure 1D and F). This implies that cells sensitive to the loss of *CDC7* are more resistant to BET-inhibition and vice versa. Since the effects of BET-inhibitors can be highly cell type specific, we explored if a similar pattern could be observed in other cancer types[22]. While we found a negative correlation of pre-RC gene expression with sensitivity to BET-inhibitors in colorectal cancer, we did not find a correlation between the sensitivity to *CDC7* loss by CRISPR/CAS9 and the sensitivity to BET-inhibitors (Supp. Figure 1A-D), indicating that this is a tumor type specific phenomenon. While the sensitivity towards BET-inhibitors have been linked to MYC expression in various cancer types, we did not observe such a connection in ovarian cancer cell lines in contrast to melanoma, non-small cell lung cancer or renal cell carcinoma (Figure 1D, Supp. Figure 1D, E)[12].

In summary, our results indicate a mutual dependency between the expression of pre-RC genes and the sensitivity towards BET-inhibitors in ovarian cancer.

Synergistic effects of AZD5153 with XL413

Based on our findings, indicating a link between the pre-RC expression and the sensitivity to BET-inhibitors, we investigated whether knocking down pre-RC genes by siRNA would alter the sensitivity of ovarian cancer cells to BRD4 inhibitors.

We utilized the BET-inhibitor AZD5153 (BRD4i) alongside siRNA targeting either *MCM7* or the licensing factor *CDT1*, both of which, along with *CDC6* play critical roles in the formation of the

pre-replication complex. Our results showed a significant sensitization to AZD5153 in cells treated with *CDT1* siRNA, while *MCM7* siRNA treatment resulted in a more modest sensitization (Figure 2A, B).

To further explore the potential of modulating replication origins and initiation as a strategy to enhance the efficacy of AZD5153, we conducted pre-treatment experiments using drugs that impact pre-replication proteins or replication initiation. Specifically, we used RL5a, a compound known to reduce the expression of the pre-RC genes *MCM2-7*[23]. Following a 72-hour pre-treatment with RL5a, we observed increased sensitivity to AZD5153 in OVCAR4 and OVCAR8 cells, while no sensitization was observed in OVSAHO, OVCAR3, and COV318 cells (Figure 2C, D).

Additionally, we examined the effects of statins, which have been reported to decrease MCM protein levels[24,25]. Pre-treatment with simvastatin sensitized OVCAR4, OVCAR8, and OVSAHO cells to AZD5153; however, the synergistic effect was only observed within a narrow concentration window of simvastatin. Notably, some cell lines, such as OVCAR8, exhibited high sensitivity to simvastatin on its own (Figure 2E, F). In contrast, the CDC7 inhibitor XL413, which disrupts the phosphorylation of MCM2 and its replication origin activation, demonstrated a robust synergistic effect across a wide range of concentrations in all tested cell lines (Figure 2G-I)[26].

The synergistic effects are partially dependent on TP53 mutation

Next, we examined whether this synergistic effect could also be observed in immortalized fallopian tube cell lines[27]. To our surprise, all four tested cell lines exhibited strong synergy when pre-treated with various concentrations of the CDC7 inhibitor XL413, followed by the addition of the BET inhibitor AZD5153 (Figure 3A). Importantly, these fallopian tube cell lines were immortalized by inhibiting the *TP53* gene either through the expression of the SV40 Large T antigen (in FT189) or via shRNA-mediated knockdown of P53 (in FT237, FT240, and FT246). To determine if the synergistic effects depend on the disruption of the *TP53* pathway, we utilized a panel of primary ovarian cancer cell lines. These lines either contained accumulated P53 (indicating a *TP53* mutation - MA1-MA6 and MA11) or expressed normal P53 levels (MA7, MA8, MA9, MA10 and MA12) (Figure 3B). We found that the synergistic effect of XL413 and AZD5153 was observed only in the cell lines with accumulated P53, which is indicative of mutated *TP53* (Figure 3B, C). Since the primary cell lines that were not affected by the combinational treatment also lacked PAX8 expression, a marker for high-grade serous carcinomas (HGSC), we could not rule out the possibility that the observed effect might be subtype-specific for reasons other than TP53 disruption (Figure 3B). To further investigate this, we used HeyA8 cells, which express wild type P53 and only show a weak sensitization to AZD5153 when treated with XL413 (Figure 3D). Upon P53 knockdown using siRNA we observed a marked enhancement of the synergistic effect between XL413 and AZD5153, resulting in a 100-fold increase in sensitivity to AZD5153. This indicates that the synergy is indeed dependent on the loss of *TP53* (Figure 3D).

We also explored if the expression of other genes such as cyclin E1, (*CCNE1*) influences the synergistic effect. *CCNE1* is frequently amplified in HGSCs (20%) and its overexpression has been shown to disrupt the origin loading[28–30]. We employed the immortalized fallopian tube cell line FT282, which expresses shRNA against *TP53* as well as an inducible *CCNE1* vector. While

we observed a synergistic effect in cells with normal cyclin E1 levels, this synergy was significantly enhanced in cells overexpressing cyclin E1 (Figure 3E).
Lastly, when analyzing the effects on DNA damage signaling, we observed a strong increase phosphorylated yH2AX (p-yH2AX) in cyclin E1 overexpressing cells following double treatment, while levels of 53BP1 decreased (Figure 3F).
These findings suggest that the synergistic effects of XL413 and AZD5153 are partially dependent on TP53 status and may be influenced by the expression of genes involved in cell cycle regulation, such as cyclin E1.

Effects on DNA damage signaling pathways

To assess the impact on DNA damage signaling pathways, we examined the effects of MCM7 knock down and AZD5153 on various markers of DNA damage. Remarkably, treatment with MCM7 siRNA in conjunction with AZD5153, resulted in a significant increase in p-yH2AX levels, a key indicator of DNA damage. Additionally, we observed a decrease in nuclear 53BP1 foci staining, which represents a marker of DNA double-strand break (DSB) repair (Figure 4A) Intriguingly, MCM7 knockdown also led to a substantial increase in RAD51 foci, but this was abolished upon treatment with the BET-inhibitor. Next we tested if the combination of AZD5153 and the CDC7 inhibitor XL413 had a similar effect on DNA damage markers. In contrast to RNAi treatment, we did not observe an additive or synergistic increase in p-yH2AX with the combination treatment (Figure 4B). Similarly to the effects seen with *MCM7* RNAi, the number of 53BP1 foci decreased when comparing the combination of AZD5153 with XL413 to XL413 treatment alone (Figure 4C).
We also analyzed effects on the cell cycle and found that XL413 resulted in a strong accumulation of cells in the G1 phase due to G1 checkpoint arrest. However, this accumulation was diminished by AZD5153 treatment (Figure 4D). We next performed real-time PCR using a gene panel to determine whether other DNA damage-related genes were affected by the treatment of AZD5153 and XL413 (Figure 4E). Recent studies have shown BET-inhibitors can reduce the gene expression of several genes involved in DSB repair[14]. Our real-time PCR analysis confirmed that XL413 treatment led to the upregulation of several genes involved in double-strand break repair, including *RAD51*, *53BP1*, *RAD51D*, *POLQ*, *BARD1*, *RAD51C*, *BRCA1*, *BRCA2*, and *XRCC2* (Figure 4E). Notably, the upregulation was reversed by the addition of AZD5153. This finding aligns with our observation that while XL413 activates the serine/threonine kinase CHK1, CHK2 and ATR, this activation was abrogated by the combination with AZD5153 (Figure 4F).
To further explore replication stress in cells treated with both drugs, we performed native BrdU immunofluorescence to measure the levels of single-strand DNA (ssDNA), which serves as a marker for replication stress. Importantly, cells treated with both XL413 and AZD5153 exhibited significantly higher levels of ssDNA compared to cells treated with either agent alone or control cells (Figure 4G).
To assess if the lack of DNA damage response and continuous progression through the cell cycle leads to the accumulation of more unresolved DNA damage during the combination treatment, allowing the cells to recover in normal media for 16 hours after the standard treatment protocol (Figure 4H).

Remarkably, upon recovery, we noted a pronounced elevation in p-yH2AX, 53BP1 and RAD51, indicating that cells accumulate more DNA damage during the combination treatment.
These findings suggest that while XL413 treatment alone enhances DNA damage and DNA damage response, combining XL413 with AZD5153 exacerbates genomic instability by impairing the cells' ability to effectively respond to DNA damage and replication stress.

Reduction in origin licensing and BRD4 inhibition leads to an increase in R-loops

Recent studies have shown that BET-inhibition can lead to an increase in R-loop formation, which refers to DNA:RNA hybrids to occur as a result of conflicts between the transcription and the replication machinery[17,31]. Building on this knowledge, we aimed to investigate whether combinating BET-inhibition with a reduction in origin licensing or replication origins could enhance R-loop accumulation, thus elucidating the underlying mechanism behind the observed increase in replication stress.
Indeed, when treating cells with MCM7 siRNA in combination with AZD5153, we observed a significant increase in nuclear S9.6 staining, an antibody that specifically binds to RNA:DNA duplexes (Figure 5A). This effect was similarly observed across multiple cell lines when XL413 was combined with AZD5153 (Figure 5B). In contrast to findings in other studies, we noted that treatment with the BET inhibitor alone resulted in only a weak or negligible increase in R-loop formation in our analyzed cell lines[31]. Similarly, to the XL413 treatment, we also observed an increase in R-loop formation when combining RL5a with the AZD5153 (Sup-Figure 2A). We next investigated whether cyclin E1 levels influenced R-loop formation.
Using immortalized fallopian tube cell line FT282, we found that in cells expressing low levels of cyclin E1, there was no increase in R-loops upon combined treatment. In contrast, cells with high cyclin E1 expression exhibited a significant rise in R-loop levels (Figure 5C). To assess the transcription dependence of this effect, we employed Triptolide (TRP), a TFIIH inhibitor that blocks transcription initiation and leads to RNA polymerase II (*RNAPII*) degradation. Interestingly, TRP treatment reduced S9.6 nuclear fluorescence staining in cells treated with both XL413 and AZD5153 (Figure 5D). Moreover, overexpressing RNase H1, an enzyme responsible for removing R-loops, resulted in decreased R-loop formation (Figure 5E).
Recently a dual role of the MRN (Mre11, Rad50 and Nbs1) complex in R-loop formation has been suggested. On one hand, it can resolve R-loops present at the replication fork through a nucleolytic-independent mechanism. On the other hand, it can promote R-loops to facilitate the resection at DSBs and thereby enhances homologous recombination in conjunction with RNAPII[32–34]. To investigate if the increase in R-loop formation could be attributed to enhanced DNA end-resection, we pretreated the cells with the MRE11 inhibitor Mirin. Encouragingly, Mirin treatment reduced S9.6 nuclear intensity in cells subjected to the combination of AZD5153 with XL413 (Figure 5F). These results support the model that both, MRN and RNAPII, are required for R-loop induced double strand break[33]. They also align with findings that resolution of R-loops is facilitated by the homologous recombination and Fanconi armenia genes, both of which are downregulated in our model following AZD5153 treatment[35]. This is further corroborated by the research from Ohle et al, which indicates that R-loops are essential efficient HR-dependent double strand repair. We then tested whether inhibiting R-loops and the MRN complex would reduce the ability of cells to repair DSBs by HR[33]. We therefore treated the cells additionally to our combinational treatment with the MRN inhibitor Mirin or TRP before allowing the cells to

recover in normal media for 16 hours. Following Mirin treatment, we observed a significant increase in p-yH2AX foci number and nuclei intensity (Figure 5G). When analyzing the number of RAD51 and 53BP1 foci we observed that upon the treatment with mirin the cells increased 53BP1 foci numbers whereas the number RAD51 foci remained unchanged. This indicates a shift from HR DSB repair to alternative DSB repair pathways that require no DNA end-resection.
To confirm our findings, we examined if inhibiting the MRN complex or RNAPII could also decrease nuclear S9.6 in cells treated with *MCM7* or *CDT1* siRNA alongside the BRD4 inhibitor AZD5153. Indeed, inhibiting both the MRN complex or RNAPII resulted in a significant reduction in R-loop formation in cells co-treated with AZD5153 (Figure 5H). Collectively, these data demonstrate that the combined treatment of XL413 and AZD5153 promotes an increase in genomic instability that is caused by unresolved DSBs. The MRN complex together with RNAPII promotes end resection and R-loop formation that can't be resolved in the double treated cells.

Reduction in origin licensing and BRD4 inhibition effects replication fork stability

Based on the previous results we investigated the effects of combined treatment with XL413 with AZD5153 on replication fork stability using a fiber combing assay (Figure 6A). The combined treatment significantly reduced the number of ongoing replication forks by increasing fork stalling (Figure 6B). Notably, after the inhibitors were removed, there was an increase in origin firing. We also observed a significant increase in replication speed, further supporting our finding that R-loops are increased DSBs rather than at the replication fork, since previous research indicated that R-loops at the replication fork slow down replication[32] (Figure 6C).
Increased replication speed is associated with genomic instability and can occur due to either the upregulation of proteins that enhance transcription or a compensatory mechanism where increased replication speed offsets the greater distance between replication origins[36]. In contrast, fork stability was only weakly affected by the combined treatment (Figure 6D). The increase in replication speed could also be attributed partially to ATR activation following XL413 treatment when compared to control (Figure 4F).
For further analysis of fork stability, we treated cells sequentially with cIdU and IdU for 30 minutes each, followed by a high dose of 4mM hydroxyurea (HU) for 4 hours. Cells exhibiting reduced fork stability will display a lower IdU to cIdU ratio. While we observed a decreased fork stability with both XL413 alone and in combination with AZD5153, there was no significant difference between the two treatments (Figure 6E), suggesting that XL413 is the primary contributor to replication fork instability.
We next examined the ability of cells to restart replication after HU treatment. Cells subjected to the combined treatment with XL413 and AZD5153 were less capable of restarting replication (Figure 6F).
During our analysis of cells in S-phase, using the EdU incorporation assay, we found that both XL413 and the combined treatment significantly reduced the number of replicating cells (Figure 6G). However, by washing out the treatment before administering EdU, this effect was mitigated (Figure 6G). In summary, the combined treatment of XL413 and AZD5153 results in increased fork stalling and enhanced replication speed, highlighting changes in the intricate interplay of fork dynamics and genomic instability.

Discussion:

The bromodomain and extraterminal (BET) protein family, consisting of BRD2, BRD3, BRD4, and BRDT, functions as epigenetic readers that specifically recognize acetylated lysine residues on chromatin[37]. Among these proteins, BRD4 is the most extensively studied with established roles in multiple cancer types, including ovarian cancer[38–41]. Its primary role in cancer involves regulating transcription through the recruitment of critical regulatory elements[39]. Specific inhibitors which disrupt the interaction between BET proteins and chromatin have shown promising results in preclinical models[37,41].

BRD4 is intricately involved in the DNA replication stress response and regulates the pre-replication complex, which is crucial for proper intra-S phase checkpoint signaling[19]. BRD4 has been shown to interact with several components of the pre-replication complex, including MCM5, MCM7, CDC6 and CDC7.

In our study, we observed a positive correlation between BET expression and origin of replication gene expression. Moreover, analysis of the Cancer Cell Line Encyclopedia dataset, indicated that increased expression of origin of replication genes exhibited greater sensitivity to BET inhibitors, suggesting a dependency on these genes. Interestingly, this correlation was not apparent in BRD4 knockout experiments using CRISPR/CAS9, which aligns with previous research showing that the BET-inhibitor AZD5153 does not disrupt the pre-replication complex like BRD4 knockout does[19]. This in turn could contribute significantly to the sensitivity and resistance to BET inhibition. We therefore speculated that reducing the number of replication origins might sensitize cells to BET inhibitors. Indeed, our results confirmed this hypothesis: pre-treatment with siRNA targeting MCM7 or CDT1 as well as small molecules like RL5a and XL413 significantly increased sensitivity to AZD5153. Notably, the strongest synergy was observed with the CDC7 inhibitor XL413, which prevents activation of the pre-replication complex. Additionally, we found that loss of *CDC7* via CRISPR/CAS9 correlates negatively with the sensitivity towards different BET-inhibitors, particularly AZD5153.

Importantly, this synergy was markedly enhanced in cells with an inactive *TP53* pathway or elevated levels of cyclin E1, indicating a cancer cell-specific effect.

Reducing the number of replication origins increases replication stress resulting in an increased prevalence of cells in G1 phase. Echoing findings of Zhang et al. we observed a strong reduction of DNA damage signaling following the additional treatment with a BET-inhibitor both on the transcriptional and protein levels[19]. Their study demonstrated that BET inhibition reduces CHK1 activity, compromising the G2/M checkpoint and subsequently resulting in the accumulation of DNA damage[19]. This could explain the pronounced synergistic effects observed in TP53 deficient cells, as the absence of a functional G1/S checkpoint necessitates reliance on an intact G2/M checkpoint to maintain genomic integrity.

It is important to note that HGSCs commonly harbor *TP53* mutations, which are thought to be among the earliest in cancer evolution[42]. These mutations are already detected in benign precursor lesions like P53 signatures and in malignant lesions such as serous tubal intraepithelial carcinomas (STIC)[43]. Mathematical modeling indicates that it can take decades from the emergence of a *TP53* mutation to evolve into a STIC and subsequently several years to progress into a HGSC[44]. The early detection of STIC lesions or early stages of HGSC remains one of the biggest challenges. If this could be reliably achieved it would become of

interest if combination therapies like the one tested here could effectively eradicate both precursor lesions as well as advanced HGSCs.

Furthermore, we found that elevated cyclin E1 levels further increased sensitivity to the combined treatment with the CDC7 inhibitor XL413 and the BETi AZD5153 even further.

In normal cells the expression of cyclins, including cyclin E1, is tightly regulated during the cell cycle. Recent studies indicate that the origin of the replication gene ORC1 represses the expression of *CCNE1* transcriptionally, while CDC6 increases it[45]. Additionally, during the G1 phase, a CDC6 motif cooperates with cyclin E1-CDK2 to promote ORC1-CDC6 interactions[46].

Beyond direct interactions with the origin of replication complexes, aberrant expression of cyclin E1 might also influence the origin of replication indirectly by shortening G1 phase limiting the cellular capacity to establish the required number of replication origins for a successful replication during S phase.

Importantly we observed a pronounced synergistic effect in immortalized fallopian tube cells expressing high cyclin E1 levels, which was accompanied by increased R-loop formation and enhanced p-yH2AX staining. These findings suggest that the observed synergy may be specific to cancer cells. Nevertheless, synergy was identified in various tested cell lines, including those with cyclin E1 amplification (COV318, OVCAR3), gain (OVCAR4), or diploid *CCNE1* status (OVCAR8, OVSAHO), indicating that other factors likely contribute to the observed synergistic effects.

Moreover, ours and previous results indicate that reducing replication initiation by the CDC7 inhibitor XL413 limits replication under BET-inhibitor treatment, implying that BET inhibition leads to aberrant DNA replication through a mechanism dependent on CDC6-CDC7[19]. In our present study we expanded upon this concept and discovered that XL413 and AZD5153 work synergistically through distinct mechanisms of action. While the treatment with XL413 induces DNA damage and upregulates DNA repair genes, AZD5153 counteracts these effects by transcriptionally downregulating many of these DNA repair genes. Consequently, the inability of cells to repair the extensive levels of DNA damage and ultimately cell death.

Another mechanism influenced by the combination treatment with XL413 and AZD5153 is the accumulation of unresolved R-loops. Recent studies have indicated that inhibition of BRD4 results in R-loop accumulation[17,31], which manifests as the collision between the replication and transcription machinery, ultimately leading to replication stress and DNA damage. In our analysis of cancer cell lines, we observed that reducing *MCM7* expression through siRNA, as well as employing small molecules such as RL5a and XL413 in conjunction with the BET-inhibitor AZD5153 significantly increased R-loop formation. Notably, in contrast to Edwards et al, we detected only a weak or negligible increase in R-loop formation following single agent treatment with the BET-inhibitor[31].

Utilizing the TFIIH inhibitor Triptolide (TRP), which blocks transcription initiation and leads to RNAPII degradation, we observed a corresponding reduction in R-loop formation. Overexpressing RNaseH, an enzyme that degrades the RNA moiety in R-loops, similarly reduces R-loop levels. Recent studies have highlighted the dual roles for the MRN complex in R-loop formation; it can both resolve R-loops at the replication fork through a nuclease-independent mechanism and promotes R-loops to facilitate resection at double-strand breaks (DSBs), thus aiding homologous recombination (HR) in collaboration with RNAPII[32–34].

Our results support the model that MRN nuclease activity is crucial for promoting R-loops that regulate resection at DSBs[32,33,47]. Interestingly, the C-terminal binding protein interacting protein (CtIP), known to activate the MRN nuclease activity, has also been shown to suppress R-loop formation at sites of radiation damage[48]. It was further shown that inhibition of BRD4 induces HR-deficiency through the depletion of CtIP[14], indicating that the loss of CtIP could play a role in R-loop formation following BET-inhibitor treatment in our model.

Overall, the combination of molecules that target CDC7 with BET-inhibitors suggests a potential strategy that might help address cancer cells through what appears to be a synthetic lethal interaction with BET-inhibitors. While the preliminary results are encouraging, further research is needed to validate these findings across different cancer types and in more clinically relevant models.

Acknowledgements:

We thank members of the Marmé/Doberstein lab and the Department of Gynecology Mannheim for their valuable discussions and feedback. We are particularly grateful to Stefanie Gaiser from the Marmé/Doberstein lab for her technical assistance. This work was supported by the AstraZeneca iEvsion Grant.

Conflict of Interest:

K.D. and F.M. were supported for this work by the AstraZeneca iEvsion Grant.

Data Availability:

The data supporting the findings of this study are available within the article and its supplementary materials. Additional datasets generated and/or analyzed during the current study are available from the corresponding author upon reasonable request.

Ethics Statement:

This study did not involve animal subjects. However, human samples were obtained from patients undergoing surgery at the University Medical Center Mannheim with appropriate ethical approval (approval number 2011-380N-MA). Informed consent was obtained from all participants prior to sample collection.

Funding:

This work was supported by the AstraZeneca iEvsion Grant. The funding body had no role in the design of the study, data collection, analysis, interpretation, or writing of the manuscript.

Bibliography

1. Belkina AC, Denis GV. BET domain co-regulators in obesity, inflammation and cancer. *Nat Rev Cancer* 2012;12:465–77.
2. Yoshida H, Bansal K, Schaefer U, Chapman T, Rioja I, Proekt I, Anderson MS, Prinjha RK, Tarakhovsky A, Benoist C, Mathis D. Brd4 bridges the transcriptional regulators, Aire and P-TEFb, to promote elongation of peripheral-tissue antigen transcripts in thymic stromal cells. *Proc Natl Acad Sci USA* 2015;112:E4448-57.
3. Houzelstein D, Bullock SL, Lynch DE, Grigorieva EF, Wilson VA, Beddington RSP. Growth and early postimplantation defects in mice deficient for the bromodomain-containing protein Brd4. *Mol Cell Biol* 2002;22:3794–802.
4. Wessel SR, Mohni KN, Luzwick JW, Dungrawala H, Cortez D. Functional analysis of the replication fork proteome identifies BET proteins as PCNA regulators. *Cell Rep* 2019;28:3497-3509.e4.
5. Shang E, Wang X, Wen D, Greenberg DA, Wolgemuth DJ. Double bromodomain-containing gene Brd2 is essential for embryonic development in mouse. *Dev Dyn* 2009;238:908–17.
6. Gursoy-Yuzugullu O, Carman C, Price BD. Spatially restricted loading of BRD2 at DNA double-strand breaks protects H4 acetylation domains and promotes DNA repair. *Sci Rep* 2017;7:12921.
7. Liu W, Ma Q, Wong K, Li W, Ohgi K, Zhang J, Aggarwal A, Rosenfeld MG. Brd4 and JMJD6-associated anti-pause enhancers in regulation of transcriptional pause release. *Cell* 2013;155:1581–95.
8. Wang W, Tang Y-A, Xiao Q, Lee WC, Cheng B, Niu Z, Oguz G, Feng M, Lee PL, Li B, Yang Z-H, Chen Y-F, et al. Stromal induction of BRD4 phosphorylation Results in Chromatin Remodeling and BET inhibitor Resistance in Colorectal Cancer. *Nat Commun* 2021;12:4441.
9. Ibarra A, Hetzer MW. Nuclear pore proteins and the control of genome functions. *Genes Dev* 2015;29:337–49.
10. van Steensel B, Belmont AS. Lamina-Associated Domains: Links with Chromosome Architecture, Heterochromatin, and Gene Repression. *Cell* 2017;169:780–91.
11. Aird F, Kandela I, Mantis C, Reproducibility Project: Cancer Biology. Replication Study: BET bromodomain inhibition as a therapeutic strategy to target c-Myc. *eLife* 2017;6.
12. Delmore JE, Issa GC, Lemieux ME, Rahl PB, Shi J, Jacobs HM, Kastritis E, Gilpatrick T, Paranal RM, Qi J, Chesi M, Schinzel AC, et al. BET bromodomain inhibition as a therapeutic strategy to target c-Myc. *Cell* 2011;146:904–17.
13. Pérez-Salvia M, Esteller M. Bromodomain inhibitors and cancer therapy: From structures to applications. *Epigenetics* 2017;12:323–39.
14. Sun C, Yin J, Fang Y, Chen J, Jeong KJ, Chen X, Vellano CP, Ju Z, Zhao W, Zhang D, Lu Y, Meric-Bernstam F, et al. BRD4 Inhibition Is Synthetic Lethal with PARP Inhibitors

through the Induction of Homologous Recombination Deficiency. *Cancer Cell* 2018;33:401-416.e8.

15. Xu Y, Vakoc CR. Targeting Cancer Cells with BET Bromodomain Inhibitors. *Cold Spring Harb Perspect Med* 2017;7.

16. Qiu H, Jackson AL, Kilgore JE, Zhong Y, Chan LL-Y, Gehrig PA, Zhou C, Bae-Jump VL. JQ1 suppresses tumor growth through downregulating LDHA in ovarian cancer. *Oncotarget* 2015;6:6915–30.

17. Lam FC, Kong YW, Huang Q, Vu Han T-L, Maffa AD, Kasper EM, Yaffe MB. BRD4 prevents the accumulation of R-loops and protects against transcription-replication collision events and DNA damage. *Nat Commun* 2020;11:4083.

18. Maruyama T, Farina A, Dey A, Cheong J, Bermudez VP, Tamura T, Sciortino S, Shuman J, Hurwitz J, Ozato K. A Mammalian bromodomain protein, brd4, interacts with replication factor C and inhibits progression to S phase. *Mol Cell Biol* 2002;22:6509–20.

19. Zhang J, Dulak AM, Hattersley MM, Willis BS, Nikkilä J, Wang A, Lau A, Reimer C, Zinda M, Fawell SE, Mills GB, Chen H. BRD4 facilitates replication stress-induced DNA damage response. *Oncogene* 2018;37:3763–77.

20. Yu C, Mannan AM, Yvone GM, Ross KN, Zhang Y-L, Marton MA, Taylor BR, Crenshaw A, Gould JZ, Tamayo P, Weir BA, Tsherniak A, et al. High-throughput identification of genotype-specific cancer vulnerabilities in mixtures of barcoded tumor cell lines. *Nat Biotechnol* 2016;34:419–23.

21. Barretina J, Caponigro G, Stransky N, Venkatesan K, Margolin AA, Kim S, Wilson CJ, Lehár J, Kryukov GV, Sonkin D, Reddy A, Liu M, et al. The Cancer Cell Line Encyclopedia enables predictive modelling of anticancer drug sensitivity. *Nature* 2012;483:603–7.

22. Zuber J, Shi J, Wang E, Rappaport AR, Herrmann H, Sison EA, Magoon D, Qi J, Blatt K, Wunderlich M, Taylor MJ, Johns C, et al. RNAi screen identifies Brd4 as a therapeutic target in acute myeloid leukaemia. *Nature* 2011;478:524–8.

23. Gardner NJ, Gillespie PJ, Carrington JT, Shanks EJ, McElroy SP, Haagensen EJ, Frearson JA, Woodland A, Blow JJ. The High-Affinity Interaction between ORC and DNA that Is Required for Replication Licensing Is Inhibited by 2-Arylquinolin-4-Amines. *Cell Chem Biol* 2017;24:981-992.e4.

24. Li J, Liu J, Liang Z, He F, Yang L, Li P, Jiang Y, Wang B, Zhou C, Wang Y, Ren Y, Yang J, et al. Simvastatin and Atorvastatin inhibit DNA replication licensing factor MCM7 and effectively suppress RB-deficient tumors growth. *Cell Death Dis* 2017;8:e2673.

25. Liang Z, Li W, Liu J, Li J, He F, Jiang Y, Yang L, Li P, Wang B, Wang Y, Ren Y, Yang J, et al. Simvastatin suppresses the DNA replication licensing factor MCM7 and inhibits the growth of tamoxifen-resistant breast cancer cells. *Sci Rep* 2017;7:41776.

26. Sasi NK, Tiwari K, Soon F-F, Bonte D, Wang T, Melcher K, Xu HE, Weinreich M. The potent Cdc7-Dbf4 (DDK) kinase inhibitor XL413 has limited activity in many cancer cell lines and discovery of potential new DDK inhibitor scaffolds. *PLoS ONE* 2014;9:e113300.

27. Karst AM, Drapkin R. Primary culture and immortalization of human fallopian tube secretory epithelial cells. *Nat Protoc* 2012;7:1755–64.

28. Chuang L-C, Teixeira LK, Wohlschlegel JA, Henze M, Yates JR, Méndez J, Reed SI. Phosphorylation of Mcm2 by Cdc7 promotes pre-replication complex assembly during cell-cycle re-entry. *Mol Cell* 2009;35:206–16.

29. Ekholm-Reed S, Méndez J, Tedesco D, Zetterberg A, Stillman B, Reed SI. Deregulation of cyclin E in human cells interferes with prereplication complex assembly. *J Cell Biol* 2004;165:789–800.

30. Ekholm SV, Zickert P, Reed SI, Zetterberg A. Accumulation of cyclin E is not a prerequisite for passage through the restriction point. *Mol Cell Biol* 2001;21:3256–65.

31. Edwards DS, Maganti R, Tanksley JP, Luo J, Park JJH, Balkanska-Sinclair E, Ling J, Floyd SR. BRD4 Prevents R-Loop Formation and Transcription-Replication Conflicts by Ensuring Efficient Transcription Elongation. *Cell Rep* 2020;32:108166.

32. Chang EY-C, Tsai S, Aristizabal MJ, Wells JP, Coulombe Y, Busatto FF, Chan YA, Kumar A, Dan Zhu Y, Wang AY-H, Fournier L-A, Hieter P, et al. MRE11-RAD50-NBS1 promotes Fanconi Anemia R-loop suppression at transcription-replication conflicts. *Nat Commun* 2019;10:4265.

33. Ohle C, Tesorero R, Schermann G, Dobrev N, Sinning I, Fischer T. Transient RNA-DNA Hybrids Are Required for Efficient Double-Strand Break Repair. *Cell* 2016;167:1001-1013.e7.

34. Paulsen RD, Soni DV, Wollman R, Hahn AT, Yee M-C, Guan A, Hesley JA, Miller SC, Cromwell EF, Solow-Cordero DE, Meyer T, Cimprich KA. A genome-wide siRNA screen reveals diverse cellular processes and pathways that mediate genome stability. *Mol Cell* 2009;35:228–39.

35. García-Rubio ML, Pérez-Calero C, Barroso SI, Tumini E, Herrera-Moyano E, Rosado IV, Aguilera A. The Fanconi Anemia Pathway Protects Genome Integrity from R-loops. *PLoS Genet* 2015;11:e1005674.

36. Maya-Mendoza A, Moudry P, Merchut-Maya JM, Lee M, Strauss R, Bartek J. High speed of fork progression induces DNA replication stress and genomic instability. *Nature* 2018;559:279–84.

37. Shi J, Vakoc CR. The mechanisms behind the therapeutic activity of BET bromodomain inhibition. *Mol Cell* 2014;54:728–36.

38. Baratta MG, Schinzel AC, Zwang Y, Bandopadhayay P, Bowman-Colin C, Kutt J, Curtis J, Piao H, Wong LC, Kung AL, Beroukhim R, Bradner JE, et al. An in-tumor genetic screen reveals that the BET bromodomain protein, BRD4, is a potential therapeutic target in ovarian carcinoma. *Proc Natl Acad Sci USA* 2015;112:232–7.

39. Chiang C-M. Brd4 engagement from chromatin targeting to transcriptional regulation: selective contact with acetylated histone H3 and H4. *F1000 Biol Rep* 2009;1:98.

40. Rhyasen GW, Yao Y, Zhang J, Dulak A, Castriotta L, Jacques K, Zhao W, Gharahdaghi F,

Hattersley MM, Lyne PD, Clark E, Zinda M, et al. BRD4 amplification facilitates an oncogenic gene expression program in high-grade serous ovarian cancer and confers sensitivity to BET inhibitors. *PLoS ONE* 2018;13:e0200826.

41. Rhyasen GW, Hattersley MM, Yao Y, Dulak A, Wang W, Petteruti P, Dale IL, Boiko S, Cheung T, Zhang J, Wen S, Castriotta L, et al. AZD5153: A Novel Bivalent BET Bromodomain Inhibitor Highly Active against Hematologic Malignancies. *Mol Cancer Ther* 2016;15:2563–74.

42. Cancer Genome Atlas Research Network. Integrated genomic analyses of ovarian carcinoma. *Nature* 2011;474:609–15.

43. Shih I-M, Wang Y, Wang T-L. The origin of ovarian cancer species and precancerous landscape. *Am J Pathol* 2021;191:26–39.

44. Labidi-Galy SI, Papp E, Hallberg D, Niknafs N, Adleff V, Noe M, Bhattacharya R, Novak M, Jones S, Phallen J, Hruban CA, Hirsch MS, et al. High grade serous ovarian carcinomas originate in the fallopian tube. *Nat Commun* 2017;8:1093.

45. Hossain M, Stillman B. Opposing roles for DNA replication initiator proteins ORC1 and CDC6 in control of Cyclin E gene transcription. *eLife* 2016;5.

46. Hossain M, Bhalla K, Stillman B. Multiple, short protein binding motifs in ORC1 and CDC6 control the initiation of DNA replication. *Mol Cell* 2021;81:1951-1969.e6.

47. Cohen S, Puget N, Lin Y-L, Clouaire T, Aguirrebengoa M, Rocher V, Pasero P, Canitrot Y, Legube G. Senataxin resolves RNA:DNA hybrids forming at DNA double-strand breaks to prevent translocations. *Nat Commun* 2018;9:533.

48. Makharashvili N, Arora S, Yin Y, Fu Q, Wen X, Lee J-H, Kao C-H, Leung JW, Miller KM, Paull TT. Sae2/CtIP prevents R-loop accumulation in eukaryotic cells. *eLife* 2018;7.

Figure legends:

Figure 1: BET-inhibitor sensitivity and origin loading. A) Heatmap analysis of BRD genes and origin of replication genes in the ovarian cancer dataset of the TCGA data. B) Expression of origin of replication genes in patients expressing high or low levels of BRD genes. C) Ovarian cancer cell line gene expression from the CCLE dataset and dependency scores of different BRD inhibitors and CRISPR dependency score from the PRISM dataset. A low dependency score indicates a higher sensitivity. D) Correlation matrix from the data from C. E) Individual values of ORC1, MCM2, MCM4, MCM7 and CDC7 expression against the PRISM dependency score of AZD5153, CPI.0610, JQ1 and OTX015. Depicted are pearson correlations with the corresponding p-values. F) Individual values of the CDC7 CRISPR dependency score against the PRISM dependency score of AZD5153, JQ1, I.BET151, OTX015, PFI.1 and CPI.0610. Depicted are pearson correlations with the corresponding p-values.

Figure 2: Synergistic effects of AZD5153 with RL5a, Simvastatin and XL413. A) Western blot analysis of OVSAHO, OVCAR8 and OVCAR4 cells treated with control siRNA or siRNA targeting CDT1 or MCM7. Blots were probed against CDT1, MCM7 and GAPDH. B) Relative survival in cells described in a) and treated with different concentrations of the BRD4i AZD5153 for 96 hours. C) Representative western blot analysis of OVCAR8 cells treated with control or RL5a (1μM and 5μM) for 72 hours. Blots were probed against MCM7 and GAPDH. D) Relative survival in cells described in C) and pre-treated with 5μM RL5a. After 72 hours treatment with RL5a the cells were treated with different concentrations of the BRD4i AZD5153 for 96 hours before survival was measured. E) Representative western blot analysis of OVCAR8 cells treated with control or simvastatin (0.5μM and 1μM) for 72 hours. Blots were probed against MCM7 and GAPDH. F) Relative survival in cells pre-treated as described in E). After 72 hours treatment with simvastatin cells were treated with different concentrations of the BRD4i AZD5153 for 72 hours before survival was measured. G) Representative western blot analysis of OVCAR8 cells treated with control or XL413 (10μM and 20μM) for 72 hours. Blots were probed against P-MCM2, MCM2 and GAPDH. H) Relative survival in cells pre-treated as described in G. After 72 hours treatment with XL413 cells were treated with different concentrations of the BRD4i AZD5153 for 72 hours before survival was measured. I) Depicted are synergy blots with calculated HSA synergy scores from the samples shown in H).

Figure 3: The synergistic effects are partially dependent on TP53 mutation. A) Upper panel: Relative survival of FT189, FT237, FT240 and FT246 cells after pre-treatment with 10μM or 20μM XL413 for 72 hours before adding different concentrations of the BRD4i AZD5153. Lower panel: HSA synergy analysis of corresponding cell lines in the upper panel. B) Western blot analysis of a panel of primary cell lines and analyzed for PAX8, EPCAM, P53 and GAPDH. C) Relative survival of primary cells from b) pre-treated with 10μM XL413, followed by the treatment of 0.1μM AZD5153 for each 72 hours. D) Upper panel: Relative survival of HEYA8 cells that were treated with control or siRNA against P53 after pre-treatment with 10μM or 20μM XL413 for 72 hours before adding different concentrations of the BRD4i AZD5153. Lower panel:

HSA synergy analysis of corresponding cell lines in the upper panel. E) Upper panel: Relative survival of FT282 cells that express normal or high levels of Cyclin E1 (CCNE1) after pre-treatment with 10μM or 20μM XL413 for 72 hours before adding different concentrations of the BRD4i AZD5153. Lower panel: HSA synergy analysis of corresponding cell lines in the upper panel. F) Western blot analysis of samples analyzed in E) for expression of p-MCM2, MCM2 pH2AX, RAD51, 53BP1 and GAPDH.

Figure 4: Effects on DNA damage signaling pathways. A) Immunofluorescence of OVCAR8 cells treated with MCM7-siRNA followed by BRD4i treatment. Cells were analyzed and quantified for p-yH2AX (red), 53BP1 (green) and nuclear DNA (blue). RAD51 foci were additionally stained, analyzed and counted. B) p-yH2AX Immunofluorescence analysis of cells treated with XL413 followed by BRD4i treatment. C) 53BP1 Immunofluorescence analysis of cells treated with XL413 followed by BRD4i treatment. D) Cell cycle analysis of cells treated with XL413 followed by BRD4i. E) Heatmap of real time PCR analysis of cells treated with XL413 followed by BRD4i. F) Western blot analysis of OVCAR8 cells treated with XL413 followed by BRD4i. Blot was analyzed for pMCM2, MCM2, pCHK1, pCHK2, pATR, p-yH2AX, RAD51, and GAPDH. G) relative nuclear fluorescence intensity of single stranded DNA (cIdU) of OVCAR8 cells treated with XL413 followed by BRD4i treatment. H) Upper scheme: After treatment regime, cells are washed and released for 16 hours into normal media before immunofluorescence was performed. Lower panel: Analysis of foci per nuclei and integrated intensity per nuclei of p-yH2AX, 53BP1 and RAD51 in OVCAR8 cells.

Figure 5: Reduction in origin licensing and BRD4 inhibition leads to an increase in R-loops. A) Nuclear S9.6 immunofluorescence analysis of OVCAR8 cells treated with control or MCM7-siRNA followed by BRD4i treatment. B) Nuclear S9.6 immunofluorescence analysis of different cell lines treated with XL413 followed by BRD4i treatment. C) Nuclear S9.6 immunofluorescence analysis of FT282-ctrl and FT282-CCNE1 cells treated with XL413 followed by BRD4i treatment. D) Nuclear S9.6 immunofluorescence analysis of OVCAR8 cells treated with XL413 followed by BRD4i treatment. Prior to BRD4i treatment, cells were treated with the TFIIH inhibitor Triptolide (TRP) to block transcription initiation. E) Nuclear S9.6 immunofluorescence analysis of OVCAR8 cells treated with XL413 followed by BRD4i treatment. Prior to treatment, cells were transduced with a control vector or a vector expressing RNASEH1. F) Nuclear S9.6 immunofluorescence analysis of OVCAR8 cells treated with XL413 followed by BRD4i treatment. Prior to BRD4i treatment, cells were treated with Mirin or TRP. G) Immunofluorescence analysis of OVCAR8 cells treated with XL413 followed by BRD4i treatment. Prior to BRD4i treatment, cells were treated with Mirin or TRP for 48 hours before cells were washed and released into normal media for 16 hours. Cells were analyzed for p-yH2AX foci number and integrated nuclear intensity, as well as 53BP1 and RAD51 foci numbers per nucleus. H) S9.6 immunofluorescence analysis of OVCAR8 cells treated with MCM7 or CDT1-siRNA followed by BRD4i treatment. Prior to BRD4i treatment, cells were treated with TRP or Mirin.

Figure 6: Reduction in origin licensing and BRD4 inhibition affects replication fork stability. A) Left: Sketch of a replication fork treated with cIdU (red) followed by IdU (green). Below are the concentrations of the used substances in this figure. Right: A representative immunofluorescence image of a fiber spread assay with magnified fibers displayed. B) Left: treatment order of XL413 and BRD4i followed by cIdU for 40 minutes, wash steps (W) and 40 minutes of IdU treatment. Right: analyzed fibers for continuous forks, stalling forks and new origin firing. C and D) Fibers from B) were analyzed replication speed in kb/min C) and fork stability was analyzed by calculating the ratio of IdU to cIdU for each fiber D). E) Upper panel: treatment order. Lower panel: fork stability was analyzed by calculating the ratio of IdU to cIdU for each fiber. F) Upper panel: treatment order. Lower panel: fork restart was analyzed. G) Upper panel: treatment order. On the left, EdU was directly added to the cells whereas on the right cells were washed (W) before adding EdU. Lower panel: quantified EdU intensity per nucleus.

Supplementary Figure 1: Correlation analysis of different cancer types from the CCLE and the PRISM dataset

A) Cell lines were analyzed for the dependency score of AZD5153 and MCM4 expression. B) Cell lines were analyzed for the dependency score of JQ1 and MCM4 expression.Cell lines were analyzed for the dependency score of C) Cell lines were analyzed for the dependency score of AZD5153 and CDC7_CRISPR. D) Cell lines were analyzed for the dependency score of JQ1 and CDC7_CRISPR. E) Cell lines were analyzed for the dependency score of JQ1 and MYC expression. F) Cell lines were analyzed for the dependency score of AZD5153 and MYC expression.

Supplementary Figure 2: S9.6 intensity following RL5a and BRD4i treatment.

A) S9.6 Immunofluorescence analysis of OVCAR8 cells treated with RL5a followed by BRD4i treatment.

Figure 1

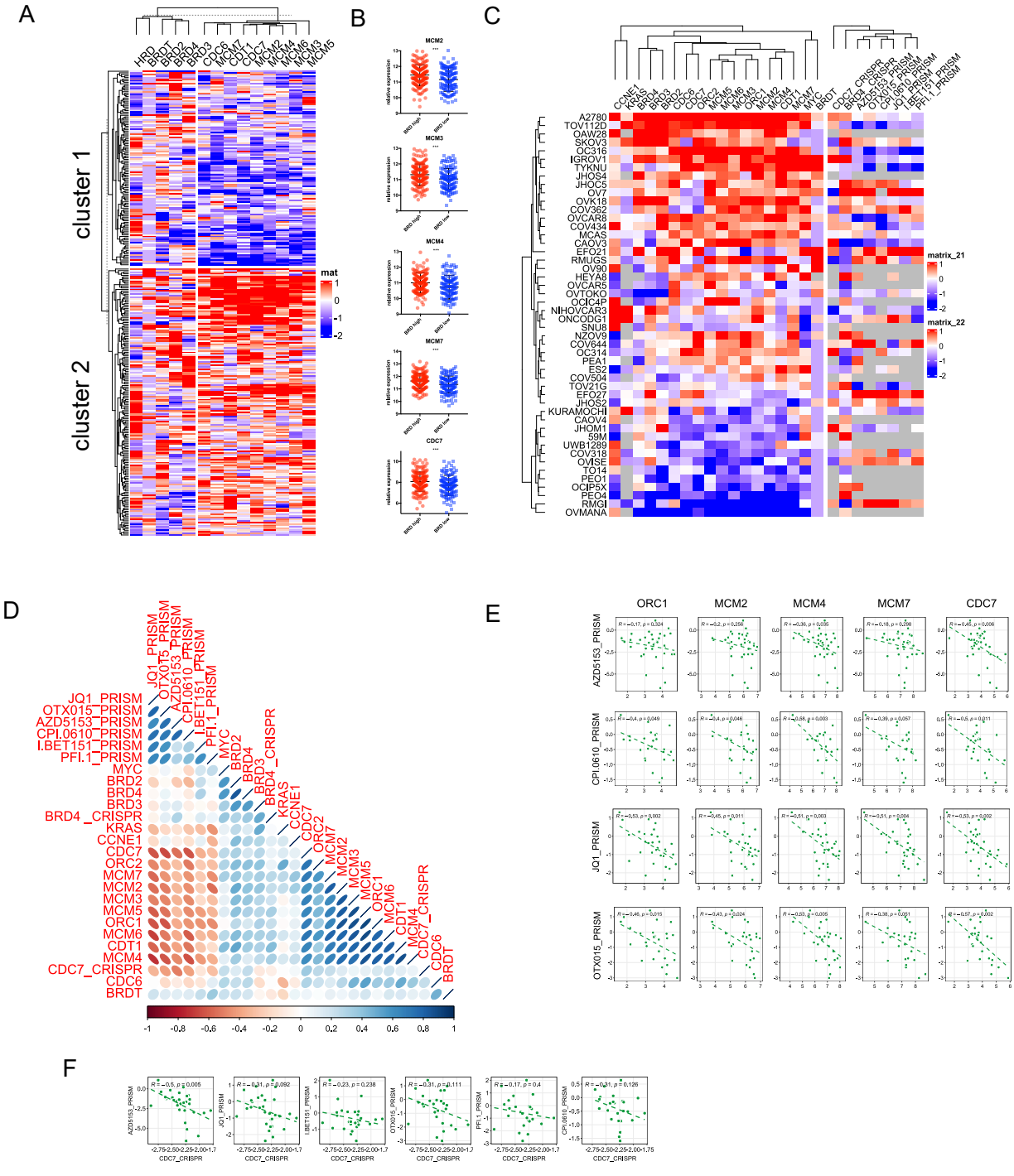
A
B
C
D
E
F
cluster 1
cluster 2
mat
MCM2
MCM3
MCM4
MCM7
CDC7
relative expression
BRD high
BRD low
matrix_21
matrix_22
ORC1
MCM2
MCM4
MCM7
CDC7
AZD5153_PRISM
CPI.0610_PRISM
JQ1_PRISM
OTX015_PRISM
CDC7_CRISPR

Figure 2

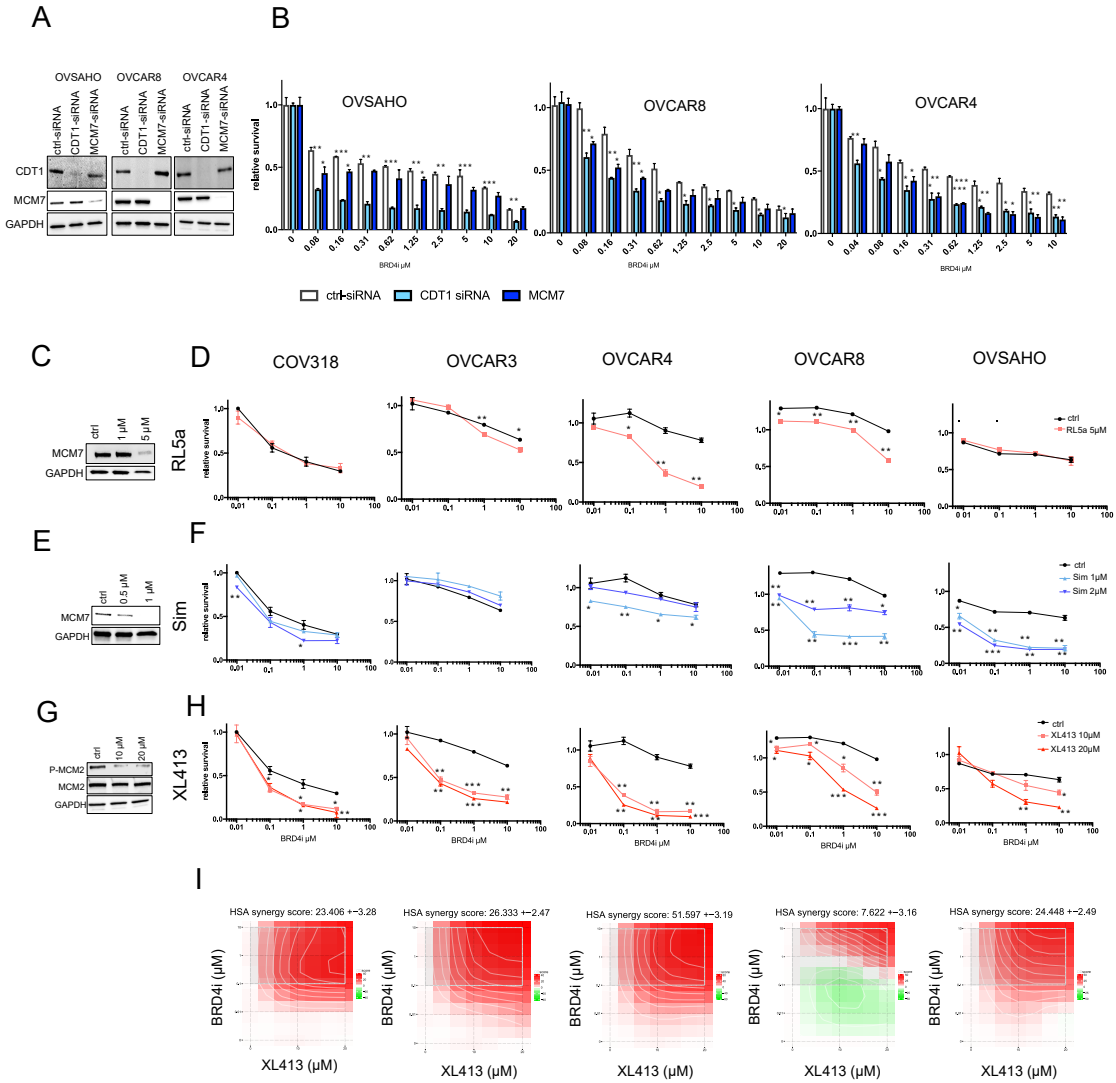
A
B
OVSAHO
OVCAR8
OVCAR4
ctrl-siRNA
CDT1-siRNA
MCM7-siRNA
CDT1
MCM7
GAPDH
relative survival
BRD4i µM
ctrl-siRNA
CDT1 siRNA
MCM7
C
D
COV318
OVCAR3
RL5a
ctrl
1 µM
5 µM
RL5a 5µM
E
F
Sim
0.5 µM
Sim 1µM
Sim 2µM
G
H
XL413
P-MCM2
MCM2
10 µM
20 µM
XL413 10µM
XL413 20µM
I
HSA synergy score: 23.406 +−3.28
HSA synergy score: 26.333 +−2.47
HSA synergy score: 51.597 +−3.19
HSA synergy score: 7.622 +−3.16
HSA synergy score: 24.448 +−2.49
BRD4i (µM)
XL413 (µM)

Figure 3

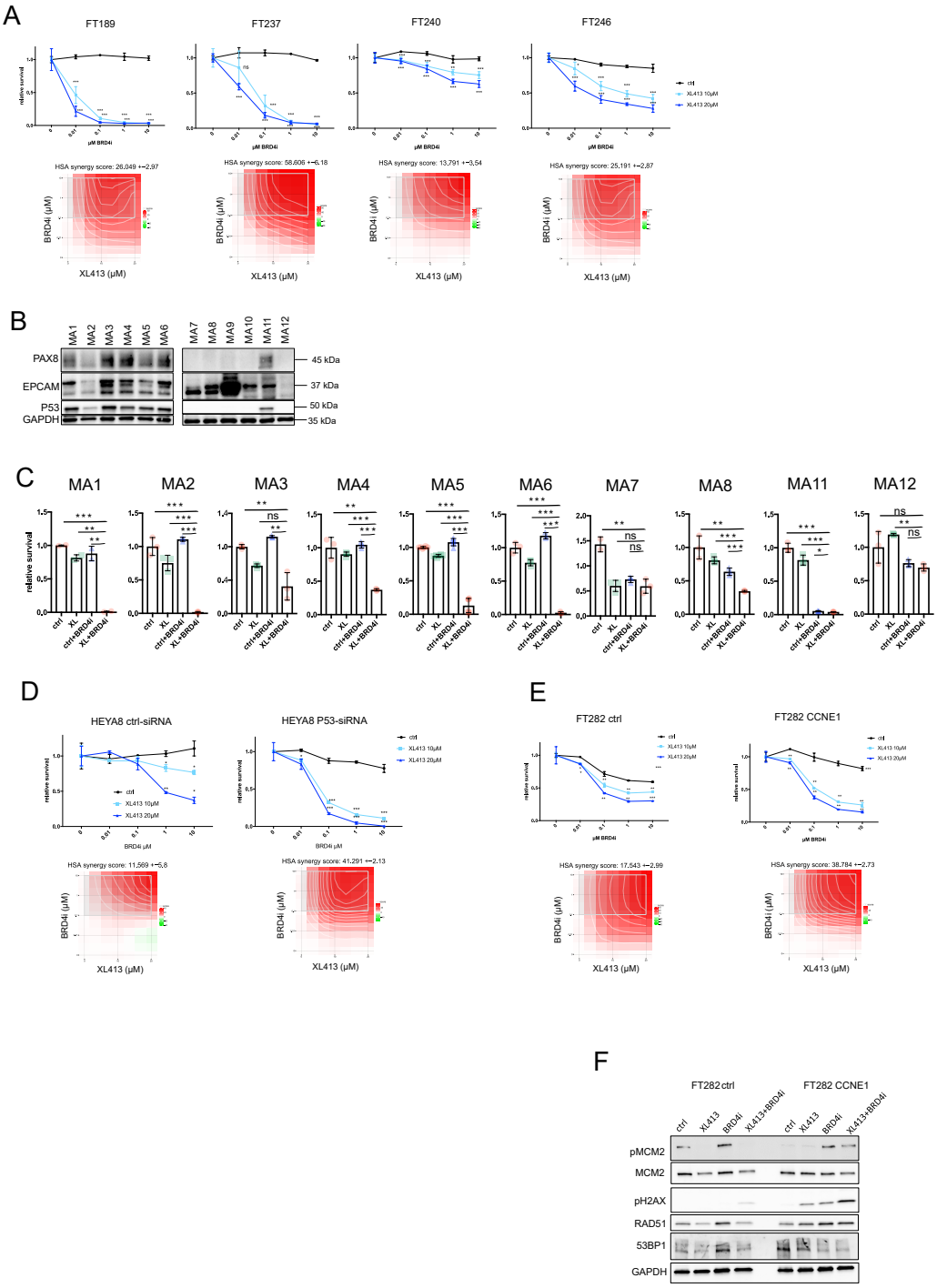
A
FT189
FT237
FT240
FT246
HSA synergy score: 26,049 +−2,97
HSA synergy score: 58,606 +−6,18
HSA synergy score: 13,791 +−3,54
HSA synergy score: 25,191 +−2,87
BRD4i (µM)
XL413 (µM)
B
MA1
MA2
MA3
MA4
MA5
MA6
MA7
MA8
MA9
MA10
MA11
MA12
PAX8
EPCAM
P53
GAPDH
45 kDa
37 kDa
50 kDa
35 kDa
C
relative survival
ctrl
XL
ctrl+BRD4i
XL+BRD4i
D
HEYA8 ctrl-siRNA
HEYA8 P53-siRNA
HSA synergy score: 11,569 +−5,8
HSA synergy score: 41,291 +−2,13
E
FT282 ctrl
FT282 CCNE1
HSA synergy score: 17,543 +−2,99
HSA synergy score: 38,784 +−2,73
F
FT282 ctrl
FT282 CCNE1
ctrl
XL413
BRD4i
XL413+BRD4i
pMCM2
MCM2
pH2AX
RAD51
53BP1
GAPDH

Figure 4

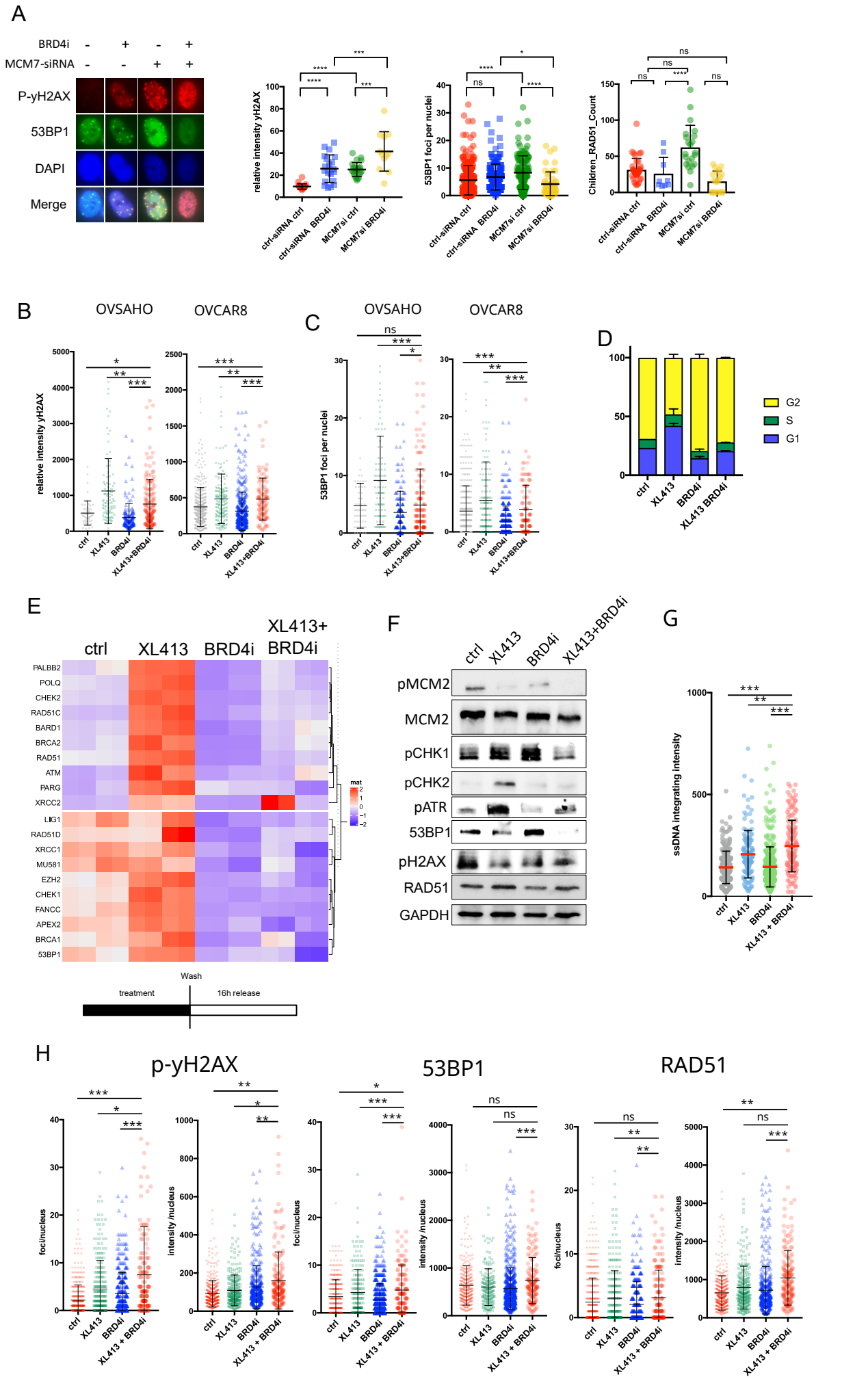
A
BRD4i
MCM7-siRNA
P-γH2AX
53BP1
DAPI
Merge
relative intensity γH2AX
53BP1 foci per nuclei
Children_RAD51_Count
ctrl-siRNA ctrl
ctrl-siRNA BRD4i
MCM7si ctrl
MCM7si BRD4i
B
OVSAHO
OVCAR8
relative intensity γH2AX
ctrl
XL413
BRD4i
XL413+BRD4i
C
OVSAHO
OVCAR8
53BP1 foci per nuclei
D
G2
S
G1
XL413 BRD4i
E
ctrl
XL413
BRD4i
XL413+ BRD4i
PALBB2
POLQ
CHEK2
RAD51C
BARD1
BRCA2
RAD51
ATM
PARG
XRCC2
LIG1
RAD51D
XRCC1
MU581
EZH2
CHEK1
FANCC
APEX2
BRCA1
53BP1
mat
Wash
treatment
16h release
F
ctrl
XL413
BRD4i
XL413+BRD4i
pMCM2
MCM2
pCHK1
pCHK2
pATR
53BP1
pH2AX
RAD51
GAPDH
G
ssDNA integrating intensity
XL413 + BRD4i
H
p-γH2AX
53BP1
RAD51
foci/nucleus
intensity /nucleus

Figure 5

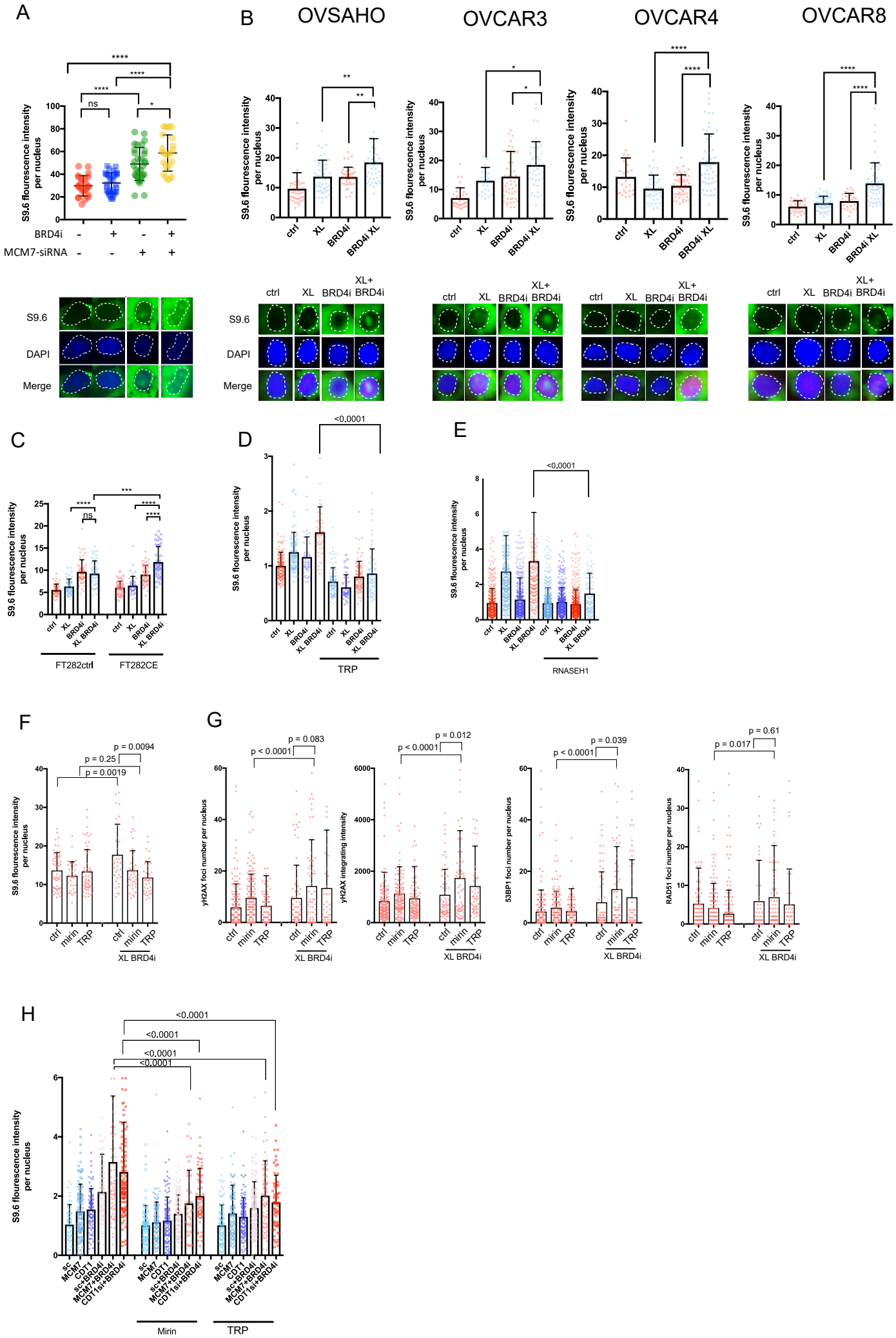
A
B
OVSAHO
OVCAR3
OVCAR4
OVCAR8
S9.6 flourescence intensity per nucleus
BRD4i
MCM7-siRNA
ctrl
XL
BRD4i
BRD4i XL
XL+ BRD4i
S9.6
DAPI
Merge
C
D
E
FT282ctrl
FT282CE
TRP
RNASEH1
F
G
p = 0.0094
p = 0.25
p = 0.0019
p < 0.0001
p = 0.083
p = 0.012
p = 0.039
p = 0.017
p = 0.61
γH2AX foci number per nucleus
γH2AX integrating intensity
53BP1 foci number per nucleus
RAD51 foci number per nucleus
mirin
XL BRD4i
H
<0.0001
sc
MCM7
CDT1
sc+BRD4i
MCM7+BRD4i
CDT1si+BRD4i
Mirin

Figure 6

A

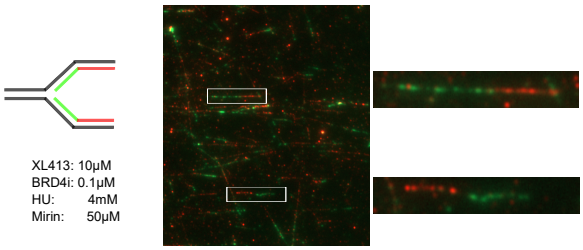

B

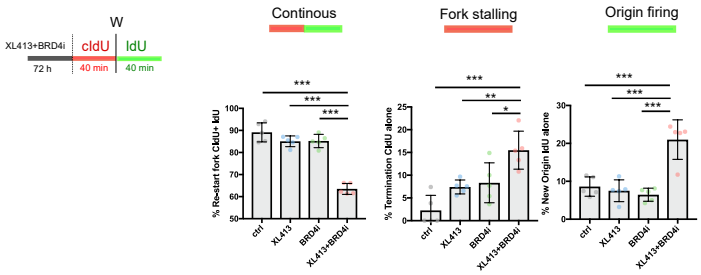

C

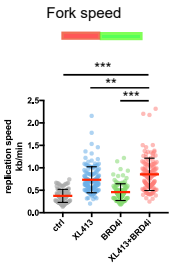

D

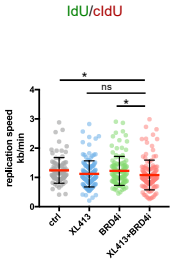

E

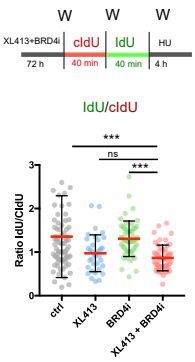

F

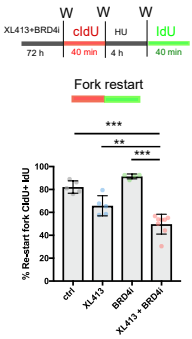

G

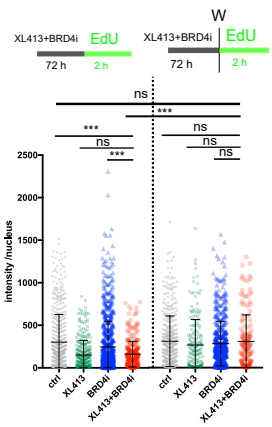

Supplementary Figure 1

A

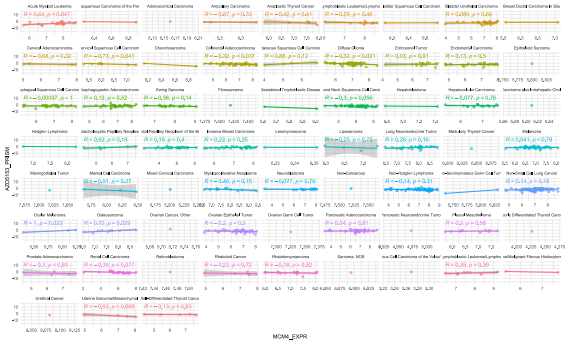

B

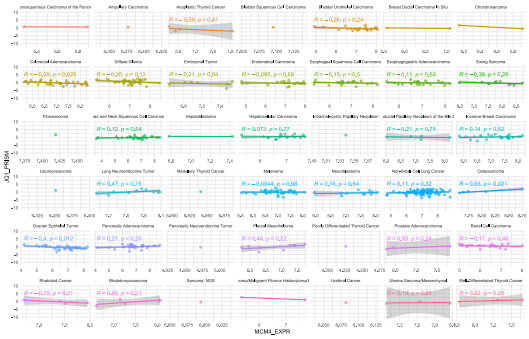

C

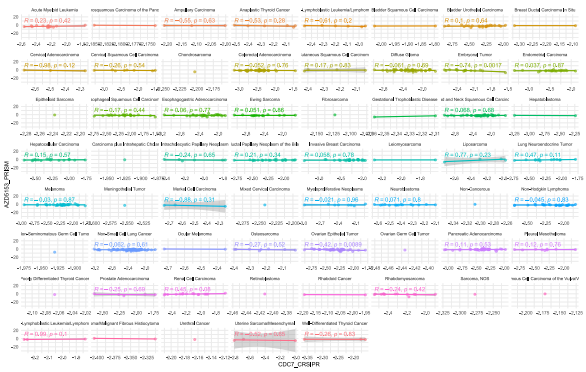

D

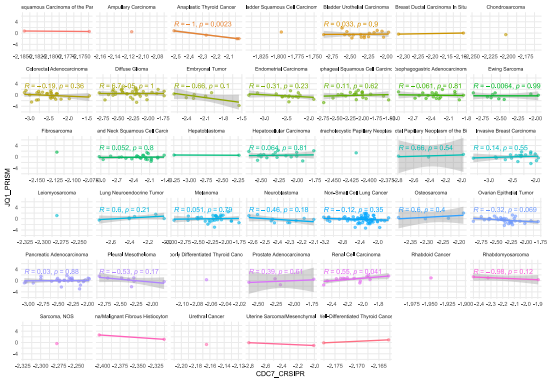

E

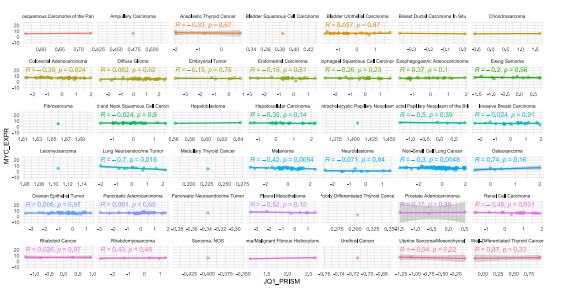

F

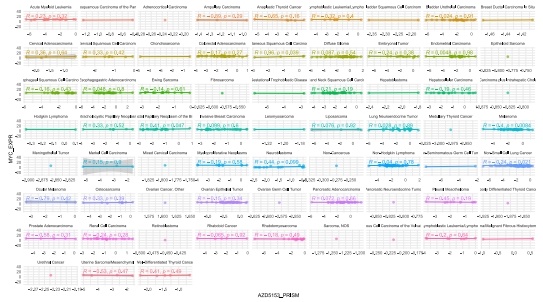

Supplementary Figure 2

A

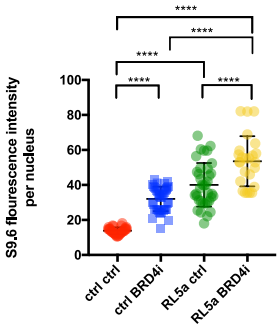

Supplementary Table S1

Antibody	Company	Number
S9.6	Sigma	MABE1095
BrdU/CIdU	Abcam	ab6326
BrdU/IdU	Becton Dickinson	347580
CDT1	CellSignaling	8064S
MCM7	CellSignaling	3735S
GAPDH	Invitrogen	14-9523-80
pMCM7	Sigma	PLA0034
PAX8	CellSignaling	59019
EPCAM	Invitrogen	PA5-79207
P53	CellSignaling	48818S
pyH2AX	Abcam	AB22551
RAD51	Abcam	ab63801
53BP1	CellSignaling	88439S
pChk1	CellSignaling	2348T
pChk2	CellSignaling	2197S
pATR	CellSignaling	2853S
MCM2	Invitrogen	PA5-32484
anti RAT Cy3	Abcam	ab98416
anti Mouse Alexa 488	Invitrogen	A11001
Anti-Rabbit Alexa 488	Invitrogen	A11034
Anti-Mouse Alexa 594	Invitrogen	A11005
Anti-Rabbit Alexa 594	Invitrogen	A11037
Goat anti Rabbit POX	Invitrogen	31466
Goat anti Mouse POX	Invitrogen	31431

Supplementary Table S2

Gene	Forward Primer (5'→3')	Reverse Primer (5'→3')
ATR	TCCCTTGAATACAGTGGCCTA	TCCTTGAAAGTACGGCAGTTC
CDK12	GCACAGTTATCAAACCTTTGGTG	CGTTCTCCCTTCGGTCTAGTT
CDKN1A (P21)	TGTCCGTCAGAACCCATGC	AAAGTCGAAGTTCCATCGCTC
CDT1	GAC ATG ATG CGT AGG CGT TTT	GAG CTG GTA ATC TGA CCT CCT
FEN1	CACCTGATGGGCATGTTCTAC	CTCGCCTGACTTGAGCTGT
GAPDH	AAT GCA TCC TGC ACC ACC AA	GTC ATT GAG AGC AAT GCC AGC
MCM7	CCTACCAGCCGATCCAGTCT	CCTCCTGAGCGGTTGGTTT
PARP11	TTTGTGGAAGCAATCTGCATTCA	GCAGCATCTCTAGCAAAATAGGT
PCNA	CCTGCTGGGATATTAGCTCCA	CAGCGGTAGGTGTCGAAGC
POLD1	CAG TGC CAA GGT GGT GTA TGG	CTT GCT GAT AAG CAG GTA TGG G
POLD2	CCA TCA GCC AAC AAT GCC AC	CTA GCC GGA AGG GTT GTG A
POLD3	GAG TTC GTC ACG GAC CAA AAC	GCC AGA CAC CAA GTA GGT AAC
POLD4_1	ATC ACT GAT TCC TAC CCG GTT	AGA GAT GCC AGA GAC TGC ACT
POLG	CATTCGTGAGAACTTCCAGGAC	GTGGGGACACCTCTCCAAG
POLH	AAGGGTGGTGGAATAATTGCAG	CTCACGAACTTGTGCCAGTAG
POLK	TGAGGGACAATCCAGAATTGAAG	CTGCACGAACACCAAATCTCC
POLQ	ACT TTT GCT GAC CAA GAT TTG CT	ACT CAT GCC AAC GAT TTG CAC
RAD17	AAAGCCCGAGGATATGCTCAT	CCAGGCAATTTTCCCGATACTT
RAD50	TTTGGTTGGACCCAATGGGG	CAGGAGGGAAATCTCCAGTACAA
TOP1MT	ACGAAGACGGGGTGAAGTG	CCGGAAAACCTCCTTTGTTGTG
TOPBP1	TTCAGCAACTCACAGTTAAGCA	GGCACACTCATACTTCTGACC
TRESLIN	CCGTGGAGCCAAAAGGATCT	GTGGAGCCGGAAACAAACAC
XRCC5	GCACTGACAATCCCCTTTCTG	TCAATGTCCTCCAGCAAATCAAA
53BP1	ATG GAC CCT ACT GGA AGT CAG	TTT CTT TGT GCG TCT GGA GAT T
APEX2	CTG GAA CAT CAA TGG GAT TCG G	CCA GCT CGT CCA AAA TGC G
ATM	ATC TGC TGC CGT CAA CTA GAA	GAT CTC GAA TCA GGC GCT TAA A
BRCA1	GAA ACC GTG CCA AAA GAC TTC	CCA AGG TTA GAG AGT TGG ACA C
BRCA2	CTG CTC GCG TTG TAC TAA CAT	TCC AAT GCA GTC ACT TAC ACA AT
BRD1	CTG CTC GCG TTG TAC TAA CAT	TCC AAT GCA GTC ACT TAC ACA AT
CDK12	GCACAGTTATCAAACCTTTGGTG	CGTTCTCCCTTCGGTCTAGTT
CHEK1	ATA TGA AGC GTG CCG TAG ACT	TGC CTA TGT CTG GCT CTA TTC TG
CHEK2	TGA GAA CCT TAT GTG GAA CCC C	ACA GCA CGG TTA TAC CCA GC
EZH2	AAT CAG AGT ACA TGC GAC TGA GA	GCT GTA TCC TTC GCT GTT TCC
FANCC	TCA AGG TCT TGG GTA TGC ACC	GCC ATT CGC CTT TGA GTG TTA AA
LIG1	GAA GGA GGC ATC CAA TAG CAG	ACT CTC GGA CAC CAC TCC ATT
MU581	AGC CCG AGT GAT ACT GCT G	TCC TCC TTG GTT AAG AAG TGG T
PALB2	AGG ATC TCT CAC CGC AGC TAA	TCA GGC CCA ACA TCA AGT GTG
PARG	AGC TTT TGG AAA GTG AAC CTC A	ATC TTC CGT AGT CTG CTT TGC
PARP1	TGGAAAAGTCCCACACTGGTA	AAGCTCAGAGAACCCATCCAC
RAD51	CAA CCC ATT TCA CGG TTA GAG C	TTC TTT GGC GCA TAG GCA ACA
RAD51C	TTT GGT GAG TTT CCC GCT GTC	AAC TTC TTT GCT AAG CTC GGA G
RAD51D	CCA GCA CTC GGA TTC TCC TG	TTG GCT GTC GGG AAG ATT TGG
XRCC1	TCA AGG CAG ACA CTT ACC GAA	TCC AAC TGT AGG ACC ACA GAG
XRCC2	ACTGCAGTAGTAGCACCCAC	TCCATTGACGCGGTCTATCC